frontiers | Frontiers in Energy Research

TYPE Original Research
PUBLISHED 06 September 2022
DOI 10.3389/fenrg.2022.996471

OPEN ACCESS

EDITED BY
Hongtao Sun,
Pennsylvania State University (PSU), United States

REVIEWED BY
Yifang Ding,
Pennsylvania State University (PSU), United States
Tao Wang,
Southeast University, China

*CORRESPONDENCE
Ting Yang,
yt-29@163.com

SPECIALTY SECTION
This article was submitted to Electrochemical Energy Conversion and Storage, a section of the journal Frontiers in Energy Research

RECEIVED 17 July 2022
ACCEPTED 02 August 2022
PUBLISHED 06 September 2022

CITATION
Xiao M, Li R, Dai Y and Yang T (2022), Hierarchically porous carbon nanofiber binder-free electrode for high-performance lithium–sulfur batteries. *Front. Energy Res.* 10:996471. doi: 10.3389/fenrg.2022.996471

Hierarchically porous carbon nanofiber binder-free electrode for high-performance lithium–sulfur batteries

Ming Xiao, Ruixue Li, Yu Dai and Ting Yang*

Collage of Materials Science and Engineering and College of Science, Central South University of Forestry and Technology, Changsha, China

It is still a challenge for lithium–sulfur (Li-S) batteries to possess high sulfur utilization and excellent electrochemical performances due to the low electrical conductivity and dissolution of polysulfides. To resolve these issues, a free-standing sulfur host composed of hierarchically porous carbon nanofibers (HPCNFs) has been synthesized via electrospinning technology. The HPCNFs with an interconnected and porous structure can facilitate electron transfer and electrolyte penetration. The mesopores in HPCNFs can provide high levels of sulfur loading, and the micropores can inhibit shuttle effects of the sulfur cathode during discharge and charge processes. After encapsulating a high mass of sulfur (76.4 wt%, HPCNFs@S), the electrode was directly applied as a cathode for the Li-S battery, which exhibited a high specific discharge capacity of 1,145 mA h g^{-1} at 0.1 C (1 C = 1,675 mA g^{-1}) and maintained 787 mA h g^{-1} after 150 charge/discharge cycles. This work provides a new insight into optimizing the electrochemical performance of Li-S batteries.

KEYWORDS

lithium–sulfur battery, cathode, carbon nanofibers, hierarchically porouss tructure, binder-free

1 Introduction

Among a variety of rechargeable batteries, lithium–sulfur (Li-S) batteries have acquired more attention as a new generation of energy storage equipment because of the high theoretical capacity (1,675 mA h g^{-1}) and low cost (Liu et al., 2021; Xiang et al., 2021; Zhong et al., 2021; Huang et al., 2022). Nevertheless, the commercialization of Li-S batteries is still hindered by the following questions: 1) the poor electrical conductivity of sulfur and Li_2S/Li_2S_2 results in low sulfur utilization; 2) polysulfides dissolved in the electrolyte and shuttled between the anode and cathode, leading to capacity decaying; 3) the volume change of sulfur causes the instability of the cathode during charging and discharging (Zhang et al., 2018a; Bian et al., 2019; Wu et al., 2020; Wang et al., 2022).

To overcome these issues, one of the most popular attempts that have been done is to design carbon nanomaterials (Liang et al., 2016; Han et al., 2017). These carbon nanomaterials have low porosity or a relatively simple pore structure. Although carbon nanomaterials improve the electrical conductivity, the adsorption of

polysulfides is not enough to limit the dissolution in long cycles (Wu et al., 2018). On the basis of the above research, porous carbon nanofibers are gradually entering into our sights (Jiang et al., 2017; Cui et al., 2020; Wang et al., 2021a). Porous carbon nanofibers have attracted much attention because of the large specific surface area and good electrical conductivity (Ge et al., 2018; Deng et al., 2021). In recent years, an effective way to alleviate polysulfides of the dissolution is to immobilize sulfur in porous carbon nanofibers (Zhou et al., 2015; Gao et al., 2019). Zhao et al. prepared the carbon nanofibers with multi-level pore structures by electrostatic spinning, and the cathode delivered an area capacity of 11.3 mA h cm^{-2} with a sulfur loading of 2.2–12.1 mg cm^{-2} (Zhao et al., 2018). Zeng et al. prepared free-standing porous carbon nanofibers with CNT-doped by electrostatic spinning, and the composite electrode showed a reversible discharge capacity of 637 mA h g^{-1} at the current density of 50 mA g^{-1} after 100 cycles (Zeng et al., 2014). Lee et al. synthesized sulfur-immobilized porous carbon nanofibers using PMMA as a pore-forming agent and activated by KOH through an electrospinning technique, and the electrode displayed a stable discharge capacity of 917 mA h g^{-1} after 300 cycles and an excellent rate performance of 859 mA h g^{-1} at the current density of 5 C (Lee et al., 2017). The porous carbon nanofibers with microporous and mesoporous structures can be used as sulfur carriers to immobilize polysulfides and alleviate volume expansion change to improve their electrochemical performances (Strubel et al., 2016; Song et al., 2017; Arie et al., 2020; Zhu et al., 2021).

At present, a large number of studies have shown that metal–organic frameworks (MOFs) can provide rich pore structures after carbonization, and the pore size of MOFs is easier to control due to the diversity of self-assembly forms of central metal ions and organic ligands (Wang et al., 2014; Skoda et al., 2019; Fang et al., 2021). This contributes to provide more room for accommodating sulfur to prevent the dissolution of polysulfides and enhance cyclic stability (Cao et al., 2020). In general, ZIFs-8 (zeolitic imidazolate frameworks) as a typical MOF material with a high specific surface area can be used as a pore-making template to adjust the size of the internal pore structure of carbon nanofibers (Liu et al., 2017; Chang et al., 2018). The ZIFs-8 material is easy to synthesize and sublimate during carbonization, and the pore structure of carbon nanofibers can be controlled by adjusting the quality of ZIFs-8 (Wang et al., 2021b). Therefore, porous carbon nanofiber electrodes with micropores and mesopores can be obtained by electrospinning technology with ZIFs-8 as a template.

Herein, in view of the above problems, hierarchically porous carbon nanofibers derived from polyacrylonitrile (PAN) have been synthesized by the electrospinning technique through thermal decomposition of ZIFs-8. The advantages of the designation are described below: 1) hierarchically porous carbon nanofibers (HPCNFs) have excellent electrical conductivity and can accelerate the electron-transfer rate; 2) HPCNFs have abundant pores to store sulfur, which can increase the adsorption of polysulfide on the carbon matrix and inhibit its shuttle effect to enhance capacity; 3) The pores of HPCNFs are beneficial to the infiltration of the electrolyte and thus increase the Li^+ transport rate. After loading sulfur (HPCNFs@S), the free-standing electrode can be directly applied as a cathode of Li-S batteries. The thermogravimetric analysis (TGA) curve showed a sulfur content of 76.4% in HPCNFs@S. Therefore, the HPCNFs@S electrode showed good electrochemical performances, which has a high initial discharge capacity of 1,145 mA h g^{-1} and still maintained a discharge capacity of 787 mA h g^{-1} after 150 cycles at 0.1 C (1 C = 1,675 mA g^{-1}). This work provides a new insight into optimizing the electrochemical performance of Li-S batteries.

2 Experimental section

2.1 Materials

Chemicals and reagents include zinc nitrate hexahydrate, 2-methylimidazole, polyacrylonitrile, N, N-dimethylformamide, sublimated sulfur, and carbon disulfide. The chemical reagents were purchased from Aladdin Shanghai Co., Ltd. The apparatuses include a beaker, rubber head dropper, reaction kettle, stirrer, magnet and oven.

2.2 Preparation of ZIFs-8

Typically, 2.625 g of $Zn(NO_3)_2{\cdot}6H_2O$ was dissolved in 100 mL of methanol to form solution A. 5.797 g of 2-methylimidazole was dissolved in another 100 mL of methanol to form solution B. Next, solution A was rapidly poured into solution B to obtain a clear white solution. The mixture was standing 2 h at room temperature after vigorous stirring. Then the mixture was centrifuged, washed with ethanol several times, and dried in a vacuum oven at 60 °C to collect ZIFs-8 powder.

2.3 Preparation of hierarchically porous carbon nanofibers (HPCNFs)

The HPCNFs were manufactured by an electrospinning technology. In detail, 0.7000 g of polyacrylonitrile (PAN, Kw = 150,000) and 0.7000 g of ZIFs-8 powder were dissolved in 10 mL of N, N-dimethyformamide (DMF) and stirred at room temperature for more than 24 h to form a homogeneous precursor solution. The liquid mixture was sucked into a 10 mL syringe and prepared for electrospinning. The parameters were set as follows: the distance between the syringe needle and the receiver was 17.5 cm, the liquid flow speed was 0.5 mL h^{-1}, and the working voltage was 16.8 kV. The

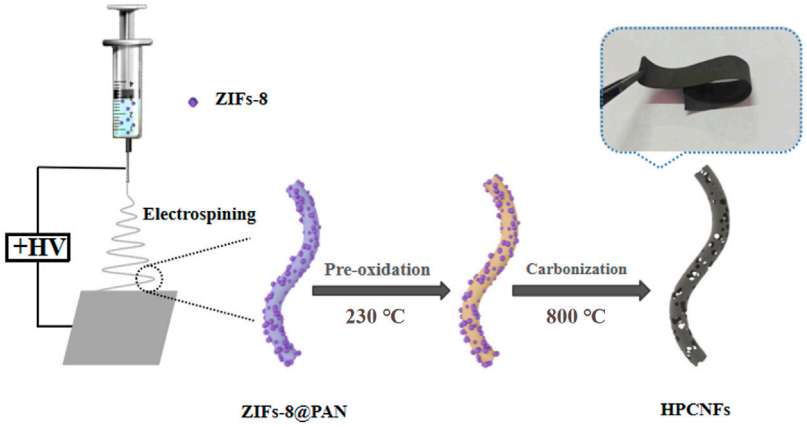

FIGURE 1
Schematic illustration for the preparation process of the HPCNFs.

obtained ZIF-8@PAN nanofibers were pre-oxidized at 230 °C for 2 h with a heating rate of 1 °C min^{-1} in an air atmosphere. Then, these stabilized nanofibers were carbonized at 800 °C for 2 h with a heating rate of 2 °C min^{-1} in an Ar atmosphere. The synthesis procedure can be seen in Figure 1. In order to compare the good electrochemical performance of HPCNFs for the Li-S battery electrode, CNFs were also prepared under the same conditions without using the ZIF-8 template.

2.4 Synthesis of HPCNFs@S materials

In a typical process, the prepared HPCNFs and sublimed sulfur were mixed in a weight ratio of 1:4 and immersed overnight in the CS_2 solvent (10 mL). Then, the mixture was dried at 60 °C to allow the CS_2 solvent to completely evaporate in the oven. Finally, the HPCNFs were heated at 155 °C for 24 h to guarantee uniform dispersion of sulfur into pores of the HPCNFs in a vacuum oven.

2.5 Material characterizations

The crystal structures of the HPCNFs and HPCNFs@S were analyzed using X-ray diffraction (XRD, Panacco X 'Pert PRO) with a 2θ range between 5° and 90° at a rate of 5 min^{-1}. The surface morphology characteristics and internal microstructure of the HPCNFs and HPCNFs@S were examined by scanning electron microscopy (SEM, SU8010) and transmission electron microscopy (TEM, FEI Tecnai F20), respectively. The nitrogen adsorption and desorption curves were used to investigate the specific surface area and pore size distribution. X-ray photoelectron spectroscopy (XPS, Thermo Kalpha) was performed to test the surface chemical composition of the S/PCNFs. The TGA curves were measured to calculate the sulfur content in the HPCNFs@S from 30 to 700 °C with a heating speed of 10 °C min^{-1} under a nitrogen atmosphere.

2.6 Electrochemical measurements

The HPCNFs@S film was clipped into 1.0 × 1.0 cm small slices and directly applied as a cathode in Li-S batteries. Lithium metal tablets were used as the anode electrode, with Celgard-2400 as the separator. 1 M lithium bis (trifluoromethanesulfonyl) imide (LiTFSI) was dissolved in 1, 2- dimethoxyethane (DME) and 1,3-dioxocyane (DOL) (1:1 by volume) with 1.0% $LiNO_3$ as the electrolyte. The ratio of the electrolyte and sulfur in each coin cell was 20 μL mg^{-1}. The batteries are assembled in an Ar-filled glovebox (H_2O/O_2 < 0.5 ppm) by using CR2025 cells. The cyclic voltammetry (CV) curves were obtained with a voltage range of 1.6–2.8 V (vs. Li^+/Li) at a scanning rate of 0.1 mV s^{-1} using a CHI760D electrochemical workstation (Chenhua Instrument Co., Ltd., Shanghai, China). A battery testing system (Neware Electronics Co., Ltd., Shenzhen, China) was used to measure the electrochemical performance of the HPCNFs@S electrode, including galvanostatic charging and discharging curves, cycling stability, and rate performances between 1.6 and 2.8 V. Electrochemical impedance spectroscopy (EIS) was carried out from 0.01 to 100 kHz.

3 Results and discussion

3.1 Structural and morphological characterizations

The micromorphologies of obtained HPCNFs and HPCHFs@S were investigated by SEM and TEM images

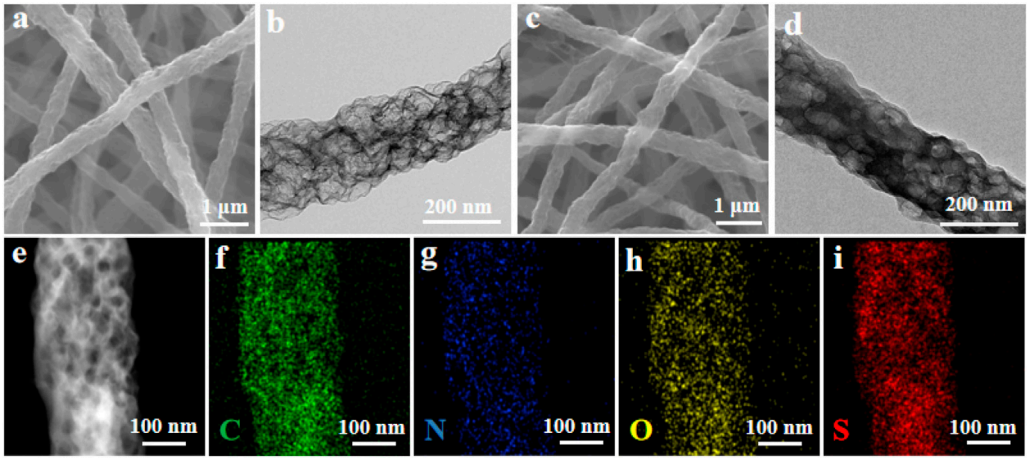

FIGURE 2
(A–B) SEM and TEM images of HPCNFs; **(C–D)** SEM and TEM images of HPCNFs@S; **(E–I)** HADDF-STEM image of HPCNFs@S and element mapping of C **(F)**, N **(G)**, O **(H)**, and S **(I)**.

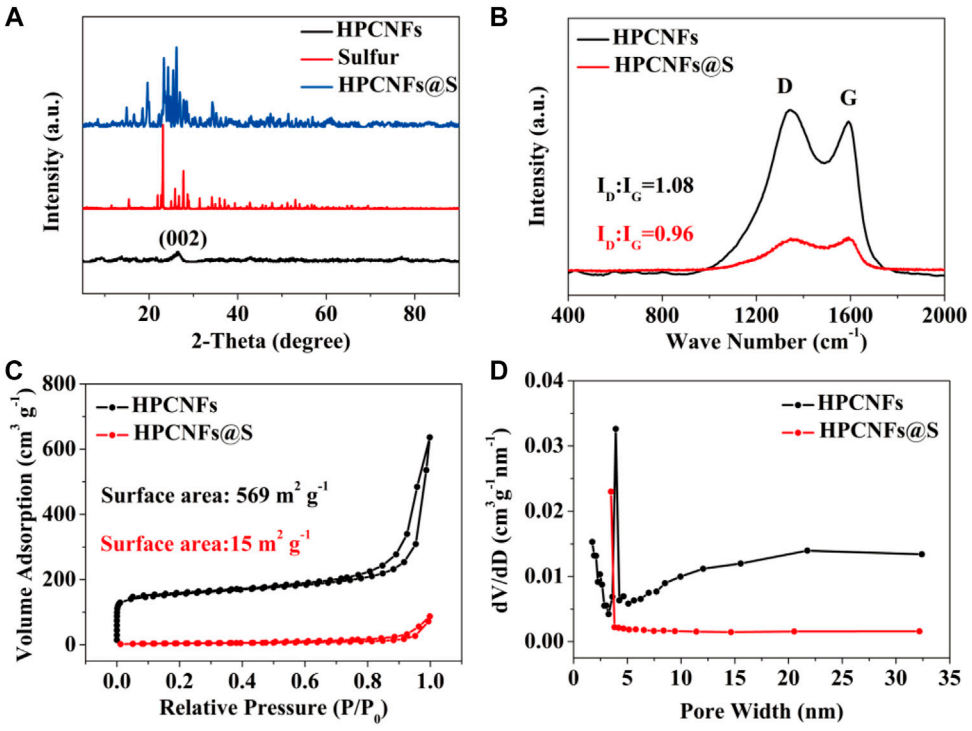

FIGURE 3
(A) XRD patterns of HPCNFs, sulfur, and HPCNFs@S; **(B)** Raman patterns of HPCNFs and HPCNFs@S; **(C)** nitrogen adsorption and desorption isotherms; **(D)** pore size distribution of the HPCNFs and HPCNFs@S.

(Figure 2). The HPCNFs exhibited interlaced nanofibers with rough surfaces and a diameter of 200 nm, forming a conductive path (Figure 2A). The porous structure of HPCNFs resulted from completely thermal decomposition ZIFs-8 particles after carbonization (Figure 2B). As shown in Figure 2C, after the sulfur infiltrated in HPCNFs, the

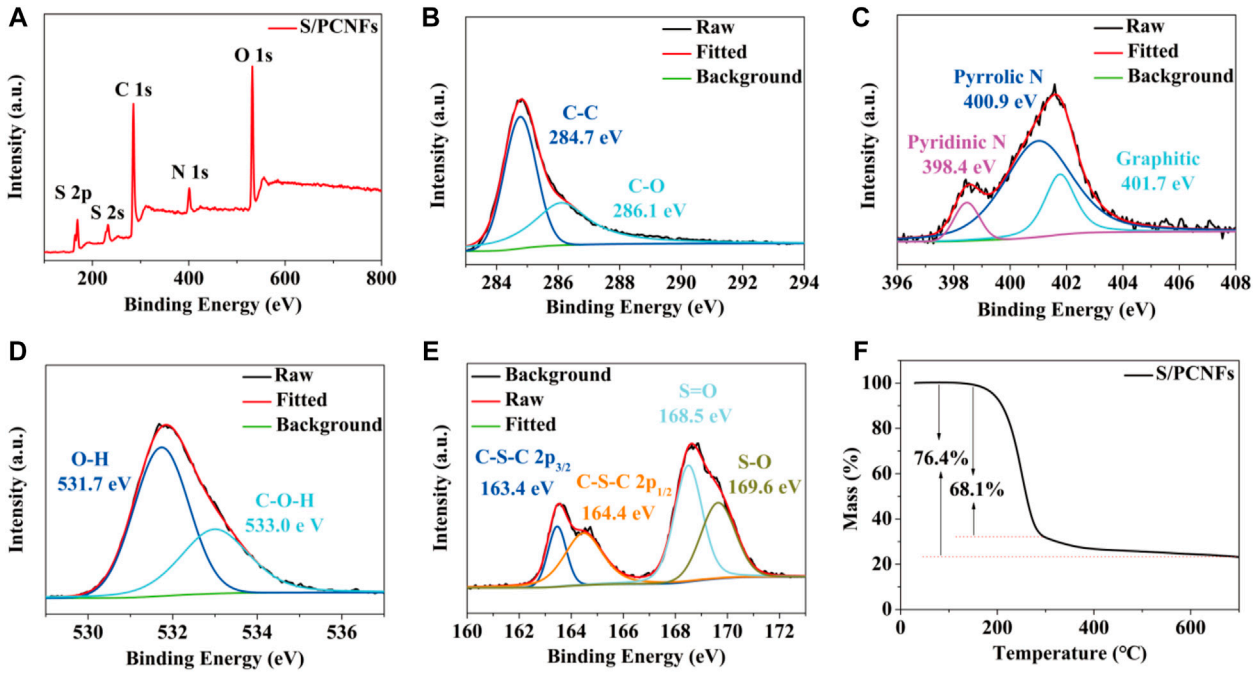

FIGURE 4
(A) XPS full and high definition: **(B)** C 1s, **(C)** N 1s, **(D)** O 1s, and **(E)** S 2p spectrum of the HPCNFs@S; **(F)** TGA curves under nitrogen.

HPCHFs@S retained its original morphology with no obvious sulfur particles, demonstrating that sulfur was uniformly filled in the micro/mesopore space of the HPCHFs@S composite (Figure 2D). The element mapping of the HPCHFs@S cathode furthered uniform dispersion of C, N, O, and S (Figures 2E–I). In addition, the HPCHFs@S cathode still has some pores after loading sulfur, which is beneficial to alleviate volume expansion during charging and discharging processes.

The X-ray diffraction (XRD) measurement was used to confirm the crystal structure of the HPCNFs@S. As shown in Figure 3A, a broad characteristic diffraction peak of the HPCNFs at 26.5° is associated with the (002) crystal plane of graphitic carbon before sulfur loading. After sulfur loading, the several different characteristic diffraction peaks of the HPCNFs@S at 2θ = 23.0°, 25.9°, 27.7°, 28.8°, and 34.2° are consistent with the pure sulfur. This shows that sulfur has been perfectly infiltrated in the HPCNFs@S, which corresponds to the SEM and TEM images. The electronic structure of the HPCNFs@S was also demonstrated by Raman spectroscopy (Figure 3B). Both samples showed two obvious Raman peaks, which were assigned to the D band of amorphous carbon at about 1,341 cm^{-1} and the G band of graphitic carbon at 1,591 cm^{-1}, respectively. In addition, the value of I_D:I_G ratio of the HPCNFs@S (I_D:I_G = 0.96) is lower than that of the HPCNFs (I_D:I_G = 1.08), which indicates that the HPCNFs@S have a higher degree of graphitization and the existence of more ordered carbon atoms (Yao et al., 2021; Zhou et al., 2021). These results were attributed to rapid electron transfer and excellent mechanical stability (Li et al., 2022).

The microporous and mesoporous structures of the HPCNFs were analyzed by nitrogen adsorption and desorption isotherms and pore size distribution. As exhibited in Figure 3C, the gas adsorption capacity increases rapidly in the low relative pressure region, revealing the presence of micropores. In addition, pores located between 2 and 35 nm are observed, indicating the existence of mesopores (Figure 3D). There is a hysteretic ring with a relative pressure of 0.0–1.0, explaining that the pore in the HPCNFs is cracked. The HPCNFs possess a higher specific surface area of 569 $m^2 g^{-1}$ and a total pore volume of 0.54 $cm^3 g^{-1}$. The large specific surface area is beneficial to accommodate high sulfur loads. After sulfur loading, the specific surface area decreases to 15 $m^2 g^{-1}$. The mesopores and micropores can make sulfur highly dispersed in HPCNFs and effectively inhibit the shuttle effect to reduce the loss of sulfur through physical adsorption (Wang et al., 2021b). The mesopores accelerate the transfer rate of lithium ions (Cao et al., 2020). The result will improve the capacity and cycling stability of the HPCNFs@S electrode.

X-ray photoelectron spectroscopy (XPS) was used to further understand the surface chemical component and chemical status of every element in the HPCNFs@S. The full spectrum of the

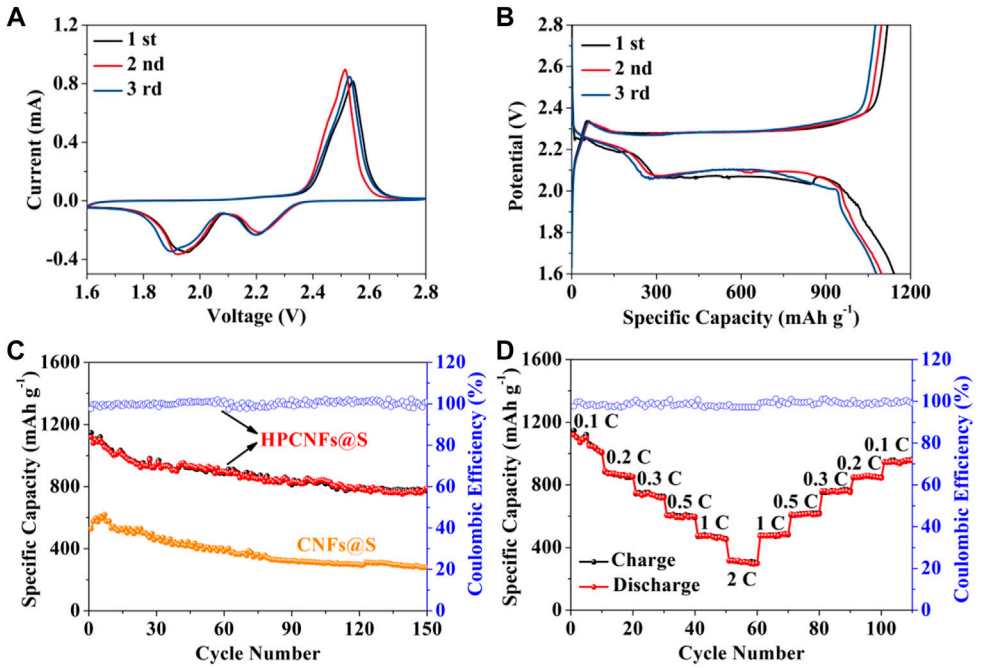

FIGURE 5
(A) CV curves of HPCNFs@S between 1.6 and 2.8 V at 0.1 mV s^{-1}; **(B)** initial three cyclic potential profiles of HPCNFs@S at 0.1 C; **(C)** cyclic performances of HPCNFs@S and CNFs@S electrodes at 0.1 C; **(D)** rate capability of HPCNFs@S at current densities from 0.1–2.0 C.

HPCNFs@S (Figure 4A) proves the existence of the four elements C, N, O, and S. As shown in Figures 4B,C the 1s peak is divided into two diverse peaks at 284.7 and 286.1 eV, belonging to C–C and C–O, respectively (Zhong et al., 2022). The high-definition spectra of the N 1s peak (Figure 4C) can illuminate the presence of pyridinic N (398.4 eV), pyrrolic N (400.9 eV), and graphitic N (401.7 eV) (Zhou et al., 2020). The polysulfides have strong physical adsorption with N, which can fully alleviate the shuttle effect, and graphitic N increases to facilitate electron transportation (Zhang et al., 2018b). The high-definition XPS scan of the O 1s peak (Figure 4D) states with two peaks, which are associated with O–H and C–O–H at 531.7 and 533.0 eV, which can limit the dissolution of polysulfides by adsorption (Zhang et al., 2018b; Wang et al., 2020a). In the S 2p spectrum of the HPCNFs@S (Figure 4E), there are two different peaks at 163.4 eV ($2p_{1/2}$) and 164.4 eV ($2p_{3/2}$), corresponding to the chemical bonds to S_8 (Wang et al., 2020b). In addition, the peak located at 168.5 and 169.6 eV was assigned to S=O and S–O due to the interaction between the oxygen group and the sulfur (Fan et al., 2021). The sulfur content in the HPCNFs@S was

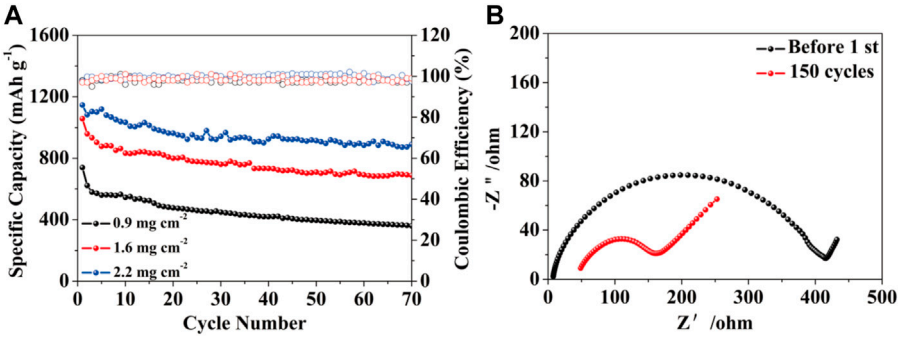

FIGURE 6
(A) Specific capacity of the HPCNFs@S electrode with sulfur loadings of 0.9, 1.6, and 2.2 mg cm^{-2}; **(B)** EIS obtained before and after 150 cycles.

measured by thermogravimetry curves (Figure 4F). Through calculations, the accurate sulfur content in the HPCNFs@S film was 76.4%, and the corresponding ratio of the sulfur and the pores was 0.29. The loss of sulfur mass consists of two parts. It was observed that the sulfur can be quickly sublimated at 155–300 °C and slowly terminated at 300 °C due to the confinement of micropores (Huang et al., 2020).

3.2 Electrochemical performance

In Figure 5A, CV curves of Li-S batteries with the HPCNFs@S film are exhibited in the potential range of 1.6–2.8 V at 0.1 mV s^{-1}. In the first cycle, a pair of reduction peaks centered at around 1.95 and 2.19 V, which are attributed to the conversion of sulfur to high-order polysulfides Li_2S_n ($4 \leq n \leq 8$) and further formation of low-order Li_2S_2 and Li_2S (Faheem et al., 2021). The oxidation peak at 2.53 V represents the formation of polysulfides Li_2S_n ($4 \leq n \leq 8$) to sulfur. The CV curve positions of the second and third cycles do not change much, indicating that the HPCNFs@S electrode has good reversibility. The charge and discharge cycle curves of the HPCNFs@S film at the current rate of 0.1 C are exhibited in Figure 5B. According to the discharge curves, there are two reduction platforms at 2.19 and 2.06 V, which are assigned to the lithiation process of sulfur, reducing soluble polysulfides and finally reducing insoluble Li_2S_2 and Li_2S. On the contrary, there is only a platform at 2.29 V corresponding to the conversion of polysulfide to sulfur. The CV curves of the HPCNFs@S are also consistent with the potential profiles. As shown in Figure 5C, the cyclic performances of Li-S batteries were further tested at 0.1 C. The HPCNFs@S film delivered an initial discharge capacity of 1,145 mA h g^{-1} and a charge capacity of 1,118 mA h g^{-1} and maintained a higher discharge capacity of 787 mA h g^{-1} and a charge capacity of 765 mA h g^{-1} after 150 cycles. However, the CNFs@S electrode only displayed 279 mA h g^{-1} after 150 cycles. The compared cyclic performances between HPCNFs@S and CNFs@S electrodes indicate that the HPCNFs@S film can store large amounts of sulfur to suppress the dissolution of polysulfides and enhance cyclic stability. Figure 5D describes the rate performances of the HPCNFs@S film at different current densities form 0.1–2.0 C. The HPCNFs@S electrode shows the large discharge capacities of 1,039, 879, 761, 616, 479, and 315 mA h g^{-1} and charge capacities of 1,035, 847, 741, 605, 459, and 299 mA h g^{-1} at 0.1, 0.2, 0.3, 0.5, 1.0, and 2.0 C, respectively. The high invertible discharge capacity of 965 mA h g^{-1} and the charge capacity of 953 mA h g^{-1} are still obtained after 100 cycles when the current density returns to 0.1 C. It is proved that the porous structure of the HPCNFs@S electrode provides abundant active sites and enhances chemisorption of polysulfides to increase capacities.

In view of the application of the HPCNFs@S electrode in Li-S batteries, it is necessary to obtain a high reversible specific capacity. As shown in Figure 6A, the HPCNFs@S electrode with a sulfur loading of 1.6 mg cm^{-2} exhibits a high specific capacity (1,145 mA h g^{-1}) and good cycling performance at 0.1 C. It is associated with the truth that the pores of HPCNFs can store more sulfur and increase the adsorption of polysulfide to prevent the dissolution in the charging and discharging processes. Figure 6B illustrates the EIS of HPCNFs@S before and after 150 cycles. The Nyquist plots are composed of a semicircle and a slanted straight line, representing the charge-transfer resistance and lithium-ion diffusion resistance, respectively. It is observed that the resistance of the HPCNFs@S electrode after 150 cycles is smaller than that before the first cycle. The reduction in the charge-transfer resistance of the sulfur cathode is relevant to the limited presence of lithium sulfide in the micropores (Li et al., 2020; Cheng et al., 2021; Wang et al., 2021c).

4 Conclusion

In summary, we prepared a hierarchical porous carbon nanofiber@sulfur composite named as HPCNFs@S by ZIFs-8 as a precursor to pore formation. The sulfur composite cathode has a large number of active sites and electron transport channels to anchor polysulfides and promote the conversion to Li_2S_2 and Li_2S. The doping of N and O also enhanced the physical adsorption of polysulfides. The HPCNFs@S electrode showed a high initial discharge capacity of 1,145 mA h g^{-1} and still remained a discharge capacity of 787 mA h g^{-1} after 150 cycles at 0.1 C. The important reasons for good electrochemical performances are as follows: 1) the crisscross conductive structure reduces electron-transfer resistance, 2) the physical adsorption to the sulfur cathode can effectively anchor polysulfides, and 3) the pore structure can accommodate the changes in sulfur volume. This work gives some guidance for rational design of the Li-S battery cathode, and it is expected to be widely used in energy storage.

Data Availability Statement

The original contributions presented in the study are included in the article/supplementary material; further inquiries can be directed to the corresponding author.

Author contributions

MX: synthesizing materials and writing the manuscript; RL: characterization of materials and writing the manuscript; YD: funding acquisition; TY: checking the manuscript and funding acquisition.

Funding

This work was supported by the National Natural Science Foundation of China (Grant No. 42007138) and the Education Department of Hunan Province (Grant No. 21C0135).

Conflict of interest

The authors declare that the research was conducted in the absence of any commercial or financial relationships that could be construed as a potential conflict of interest.

Publisher's note

All claims expressed in this article are solely those of the authors and do not necessarily represent those of their affiliated organizations or those of the publisher, the editors, and the reviewers. Any product that may be evaluated in this article or claim that may be made by its manufacturer is not guaranteed or endorsed by the publisher.

References

Arie, A. A., Kristianto, H., Cengiz, E. C., and Rezan, D. C. (2020). Preparation of salacca peel-based porous carbons by K_2CO_3 activation method as cathode materials for Li-S battery. *Carbon Lett.* 30, 207–213. doi:10.1007/s42823-019-00085-1

Bian, Z. H., Xu, Y., Yuan, T., Peng, C. X., Pang, Y. P., Yang, J. H., et al. (2019). Hierarchically designed CNF/S-Cu/CNF nonwoven electrode as free-standing cathode for lithium-sulfur batteries. *Batter. Supercaps* 2 (6), 560–567. doi:10.1002/batt.201900014

Cao, G. Q., Bi, D., Zhao, J. X., Zheng, J., Wang, Z. K., Lai, Q. X., et al. (2020). Transformation of ZIF-8 nanoparticles into 3D nitrogen-doped hierarchically porous carbon for Li-S batteries. *RSC Adv.* 10 (29), 17345–17352. doi:10.1039/C9RA10063F

Chang, Z., Ding, B., Dou, H., Wang, J., Xu, G. Y., and Zhang, X. G. (2018). Hierarchically porous multilayered carbon barriers for high-performance Li-S batteries. *Chem. Eur. J.* 24 (15), 3768–3775. doi:10.1002/chem.201704757

Cheng, J. J., Wang, Z. J., Song, H. J., Zhong, X. L., and Wang, J. B. (2021). Effects of physical properties of N-doped carbon on carbon/N-doped carbon/sulfur composite cathodes. *Ionics* 27 (8), 3271–3279. doi:10.1007/s11581-021-04097-8

Cui, G. L., Li, G. R., Luo, D., Zhang, Y. G., Zhao, Y., Wang, D. R., et al. (2020). Three-dimensionally ordered macro-microporous metal organic frameworks with strong sulfur immobilization and catalyzation for high-performance lithium-sulfur batteries. *Nano Energy* 72, 104685. doi:10.1016/j.nanoen.2020.104685

Deng, H. L., Wang, L., Li, S. Y., Zhang, M., Wang, T., Zhou, J., et al. (2021). Radial pores in nitrogen/oxygen dual-doped carbon nanospheres anode boost high-power and ultrastable potassium-ion batteries. *Adv. Funct. Mat.* 31 (51), 2107246. doi:10.1002/adfm.202107246

Faheem, M., Li, W. L., Ahmad, N., Yang, L., Tufail, M. K., Zhou, Y. D., et al. (2021). Chickpea derived Co nanocrystal encapsulated in 3D nitrogen-doped mesoporous carbon: Pressure cooking synthetic strategy and its application in lithium-sulfur batteries. *J. Colloid Interface Sci.* 585, 328–336. doi:10.1016/j.jcis.2020.11.050

Fan, B., Zhao, D. K., Xu, W., Wu, Q. K., Zhou, W., Lei, W., et al. (2021). Nitrogen-doped carbonaceous scaffold anchored with cobalt nanoparticles as sulfur host for efficient adsorption and catalytic conversion of polysulfides in lithium-sulfur batteries. *Electrochim. Acta* 383, 138371. doi:10.1016/j.electacta.2021.138371

Fang, X. Z., Jiang, Y., Zhang, K. L., Hu, G., and Hu, W. W. (2021). MOF-derived fluorine and nitrogen co-doped porous carbon for an integrated membrane in lithium-sulfur batteries. *New J. Chem.* 45 (5), 2361–2365. doi:10.1039/d0nj05912a

Gao, C., Fang, C. Z., Zhao, H. M., Yang, J. Y., Gu, Z. D., Sun, W., et al. (2019). Rational design of multi-functional CoS@rGO composite for performance enhanced Li-S cathode. *J. Power Sources* 421, 132–138. doi:10.1016/j.jpowsour.2019.03.015

Ge, X. L., Li, C. X., Li, Z. Q., and Yin, L. W. (2018). Tannic acid tuned metal-organic framework as a high-efficiency chemical anchor of polysulfide for lithium-sulfur batteries. *Electrochim. Acta* 281, 700–709. doi:10.1016/j.electacta.2018.06.010

Han, S. C., Pu, X., Li, X. L., Liu, M. M., Li, M., Feng, N., et al. (2017). High areal capacity of Li-S batteries enabled by freestanding CNF/rGO electrode with high loading of lithium polysulfide. *Electrochim. Acta* 241, 406–413. doi:10.1016/j.electacta.2017.05.005

Huang, T. L., Cao, Q., Jing, B., Wang, X. Y., Wang, D., and Liang, L. B. (2022). Towards high performance lithium-sulfur battery: Investigation on the capability of metalloid to regulate polysulfides. *Chem. Eng. J.* 430 (1), 132677. doi:10.1016/j.cej.2021.132677

Huang, Y., Gao, X. G., Han, X. P., Guang, Z. X., and Li, X. (2020). Controlled synthesis of three-dimensional porous carbon aerogel via catalysts: Effects of morphologies toward the performance of lithium-sulfur batteries. *Solid State Ionics* 347, 115248. doi:10.1016/j.ssi.2020.115248

Jiang, Y., Liu, H. Q., Tan, X. H., Guo, L. M., Zhang, J. T., Liu, S. N., et al. (2017). Monoclinic ZIF-8 nanosheet-derived 2D carbon nanosheets as sulfur immobilizer for high-performance lithium sulfur batteries. *ACS Appl. Mat. Interfaces* 9 (30), 25239–25249. doi:10.1021/acsami.7b04432

Lee, J. S., Jun, J., Jang, J., and Manthiram, A. (2017). Sulfur-immobilized, activated porous carbon nanotube composite based cathodes for lithium-sulfur batteries. *Small* 13 (12), 1602984. doi:10.1002/smll.201602984

Li, J. R., Zhou, J., Wang, T., Chen, X., Zhang, Y. X., Wan, Q., et al. (2020). Covalent sulfur embedding in inherent N, P co-doped biological carbon for ultrastable and high rate lithium-sulfur batteries. *Nanoscale* 12 (16), 8991–8996. doi:10.1039/D0NR01103G

Li, S. Y., Cao, J. H., Wang, T., Wang, L., Deng, H. L., Zhang, Q. S., et al. (2022). Intercalation and covalent bonding strategies for constructing a stable cathode for high-energy density and long-cycling potassium-organic batteries. *Chem. Eng. J.* 431, 133215. doi:10.1016/j.cej.2021.133215

Liang, G., Wu, J. X., Qin, X. Y., Liu, M., Li, Q., He, Y. B., et al. (2016). Ultrafine TiO_2 decorated carbon nanofibers as multifunctional interlayer for high-performance lithium-sulfur battery. *ACS Appl. Mat. Interfaces* 8 (35), 23105–23113. doi:10.1021/acsami.6b07487

Liu, Y. T., Liu, S., Li, G. R., Gao, X. P., and Gao, X. P. (2021). Strategy of enhancing the volumetric energy density for lithium-sulfur batteries. *Adv. Mat.* 33 (8), 2003955. doi:10.1002/adma.202003955

Liu, Y. Z., Li, G. R., Chen, Z. W., and Peng, X. S. (2017). CNT-threaded N-doped porous carbon film as binder-free electrode for high-capacity supercapacitor and Li-S battery. *J. Mat. Chem. A* 5 (20), 9775–9784. doi:10.1039/C7TA01526G

Skoda, D., Kazda, T., Munster, L., Hanulikova, B., Styskalik, A., Eloy, P., et al. (2019). Microwave-assisted synthesis of a manganese metal–organic framework and its transformation to porous MnO/carbon nanocomposite utilized as a shuttle suppressing layer in lithium–sulfur batteries. *J. Mat. Sci.* 54 (22), 14102–14122. doi:10.1007/s10853-019-03871-4

Song, X., Wang, S. Q., Bao, Y., Liu, G. X., Sun, W. P., Ding, L. X., et al. (2017). A high strength, free-standing cathode constructed by regulating graphitization and the pore structure in nitrogen-doped carbon nanofibers for flexible lithium–sulfur batteries. *J. Mat. Chem. A Mat.* 5 (15), 6832–6839. doi:10.1039/c7ta01171g

Strubel, P., Althues, H., and Kaskel, S. (2016). Zinc-salt templating of hierarchical porous carbons for low electrolyte high energy lithium-sulfur batteries (LE-LiS). *Carbon* 107, 705–710. doi:10.1016/j.carbon.2016.06.075

Wang, G., Feng, Y., Chen, J. Y., Ju, J. G., Zhang, S. P., Zhao, Y. X., et al. (2021). Mg-Al layered double hydroxides modified N-doped porous carbon nanofibers film as

cathodic interlayer for high performance Li-S batteries. *J. Alloys Compd.* 875, 160073. doi:10.1016/j.jallcom.2021.160073

Wang, J. H., Gao, L. L., Zhao, J. J., Zheng, J. D., Wang, J., and Huang, J. R. (2021). A facile *in–situ* synthesis of ZIF-8 nanoparticles anchored on reduced graphene oxide as a sulfur host for Li-S batteries. *Mat. Res. Bull.* 133, 111061. doi:10.1016/j.materresbull.2020.111061

Wang, L., Wang, T., Peng, L. L., Wang, Y. L., Zhang, M., Zhou, J., et al. (2022). The promises, challenges and pathways to room-temperature sodium-sulfur batteries. *Natl. Sci. Rev.* 9 (3), nwab050. nwab050. doi:10.1093/nsr/nwab050

Wang, T., Zhang, Q. S., Zhong, J., Chen, M. X., Deng, H. L., Cao, J. H., et al. (2021). 3D holey graphene/polyacrylonitrile sulfur composite architecture for high loading lithium sulfur batteries. *Adv. Energy Mat.* 11 (16), 2100448. doi:10.1002/aenm.202100448

Wang, W. J., Zhao, Y., Zhang, Y. G., Liu, N., and Bakenov, Z. (2020). Nickel embedded porous macrocellular carbon derived from popcorn as sulfur host for high-performance lithium-sulfur batteries. *J. Mat. Sci. Technol.* 74, 69–77. doi:10.1016/j.jmst.2020.09.032

Wang, Y., Yang, L., Chen, Y., Li, Q., Chen, C. T., Zhong, B. H., et al. (2020). Novel bifunctional separator with a self-assembled FeOOH/coated g-C_3N_4/KB bilayer in lithium-sulfur batteries. *ACS Appl. Mat. Interfaces* 12 (52), 57859–57869. doi:10.1021/acsami.0c16631

Wang, Z. Q., Dou, Z. S., Cui, Y. J., Yang, Y., Wang, Z. Y., and Qian, G. D. (2014). Sulfur encapsulated ZIF-8 as cathode material for lithium-sulfur battery with improved cyclability. *Microporous Mesoporous Mat.* 185, 92–96. doi:10.1016/j.micromeso.2013.11.011

Wu, K. S., Hu, Y., Shen, Z., Chen, R. Z., He, X., Cheng, Z. L., et al. (2018). Highly efficient and green fabrication of a modified C nanofiber interlayer for high-performance Li-S batteries. *J. Mat. Chem. A Mat.* 6 (6), 2693–2699. doi:10.1039/C7TA09641K

Wu, Z. L., Wang, L., Chen, S. X., Zhu, X. M., Deng, Q., Wang, J., et al. (2020). Facile and low-temperature strategy to prepare hollow ZIF-8/CNT polyhedrons as high-performance lithium-sulfur cathodes. *Chem. Eng. J.* 404, 126579. doi:10.1016/j.cej.2020.126579

Xiang, H. Y., Deng, N. P., Zhao, H. J., Wang, X. X., Wei, L. Y., Wang, M., et al. (2021). A review on electronically conducting polymers for lithium-sulfur battery and lithium-selenium battery: Progress and prospects. *J. Energy Chem.* 58, 523–556. doi:10.1016/j.jechem.2020.10.029

Yao, S. S., He, Y. P., Wang, Y. Q., Bi, M. Z., Liang, Y. Z., Majeed, A., et al. (2021). Porous N-doped carbon nanofibers assembled with nickel ferrite nanoparticles as efficient chemical anchors and polysulfide conversion catalyst for lithium-sulfur batteries. *J. Colloid Interface Sci.* 601, 209–219. doi:10.1016/j.jcis.2021.05.125

Zeng, L. C., Pan, F. S., Li, W. H., Jiang, Y., Zhong, X. W., and Yu, Y. (2014). Free-standing porous carbon nanofibers-sulfur composite for flexible Li-S battery cathode. *Nanoscale* 6 (16), 9579. doi:10.1039/c4nr02498b

Zhang, A. Y., Fang, X., Shen, C. F., Liu, Y. H., Seo, I. G., Ma, Y. Q., et al. (2018). Functional interlayer of PVDF-HFP and carbon nanofiber for long-life lithium-sulfur batteries. *Nano Res.* 11 (6), 3340–3352. doi:10.1007/s12274-017-1929-0

Zhang, Y. Z., Zhang, Z., Liu, S., Li, G. R., and Gao, X. P. (2018). Free-standing porous carbon nanofiber/carbon nanotube film as sulfur immobilizer with high areal capacity for lithium-sulfur battery. *ACS Appl. Mat. Interfaces* 10 (10), 8749–8757. doi:10.1021/acsami.8b00190

Zhao, X. H., Kim, M., Liu, Y., Ahn, H. J., Kim, K. W., Cho, K. K., et al. (2018). Root-like porous carbon nanofibers with high sulfur loading enabling superior areal capacity of lithium sulfur batteries. *Carbon* 128, 138–146. doi:10.1016/j.carbon.2017.11.025

Zhong, J., Wang, T., Wang, L., Peng, L. L., Fu, S. B., Zhang, M., et al. (2022). A silicon monoxide lithium-ion battery Anode with ultrahigh areal capacity. *Nano-Micro Lett.* 14 (1), 50–15. doi:10.1007/s40820-022-00790-z

Zhong, M. E., Guan, J. D., Sun, J. C., Shu, X. Q., Ding, H., Chen, L. Y., et al. (2021). A cost- and energy density-competitive lithium-sulfur battery. *Energy Storage Mat.* 41, 588–598. doi:10.1016/j.ensm.2021.06.037

Zhou, J., Chen, M. X., Wang, T., Li, S. Y., Zhang, Q. S., Zhang, M., et al. (2020). Covalent selenium embedded in hierarchical carbon nanofibers for ultra-high areal capacity Li-Se batteries. *iScience* 23 (3), 100919. doi:10.1016/j.isci.2020.100919

Zhou, J. W., Yu, X. S., Fan, X. X., Wang, X. J., Li, H. W., Zhang, Y. Y., et al. (2015). The impact of the particle size of a metal–organic framework for sulfur storage in Li–S batteries. *J. Mat. Chem. A* 3 (16), 8272–8275. doi:10.1039/c5ta00524h

Zhou, N., Dong, W. D., Zhang, Y. J., Wang, D., Wu, L., Wang, L., et al. (2021). Embedding tin disulfide nanoparticles in two-dimensional porous carbon nanosheet interlayers for fast-charging lithium-sulfur batteries. *Sci. China Mat.* 61 (11), 2697–2709. doi:10.1007/s40843-021-1669-9

Zhu, M. Y., Wang, N. N., Wang, J., Jiang, Z. N., Huang, J. R., and Liu, T. X. T. (2021). A strategy of using temporary space-holders to increase the capacity for Li S batteries. *J. Electroanal. Chem. (Lausanne).* 882, 115008. doi:10.1016/j.jelechem.2021.115008